Journal of Organometallic Chemistry 891 (2019) 54–63

Contents lists available at ScienceDirect

Journal of Organometallic Chemistry

journal homepage: www.elsevier.com/locate/jorganchem

Versatile coordination modes of benzothiazole hydrazone derivatives towards Ru(II), Rh(III) and Ir(III) complexes and their reactivity studies with azides and activated alkynes

Lincoln Dkhar [a], Werner Kaminsky [b], Krishna Mohan Poluri [c], Mohan Rao Kollipara [a, *]

[a] Centre for Advanced Studies in Chemistry, North-Eastern Hill University, Shillong, 793 022, India
[b] Department of Chemistry, University of Washington, Seattle, WA, 98195, USA
[c] Department of Biotechnology and Centre for Nanotechnology, Indian Institute of Technology Roorkee, Roorkee, 247 667, India

ARTICLE INFO

Article history:
Received 24 January 2019
Received in revised form
10 March 2019
Accepted 10 April 2019
Available online 17 April 2019

Keywords:
Rhodium
Iridium
Arylhydrazones
Benzothiazole
Activated alkynes

ABSTRACT

Metal precursors of the type $[(p\text{-cymene})RuCl_2]_2$ and $[Cp^*MCl_2]_2$ (M = Rh/Ir) on reacting with benzothiazole hydrazones ligands (L1 = benzylidenehydrazinyl benzothiazole, L2 = 4-flourobenzylidenehydrazinyl benzothiazole and L3 = 4-methylbenzylidenehydrazinyl benzothiazole) in the ratio of 1:2 (M:L), leads to the formation of range of complexes. In the case of ruthenium precursor with ligand L1, a cationic complex $[(p\text{-cymene})Ru\{\kappa^2_{(NN')}L1\}Cl]Cl$ (**1**) is formed whereas with L2 and L3 neutral complexes $[(p\text{-cymene})Ru\{\kappa^2_{(NN')}L2/L3\}Cl_2]$ (**4** and **7**) are obtained. Rhodium precursor with L1 and L2 forms mono dentate neutral complexes $[Cp^*Rh\{\kappa^1_{(N)}L1/L2\}Cl_2]$ (**2** and **5**) while with L3 bidentate NN′ bonding complex $[Cp^*Rh\{\kappa^1_{(NN')}L3\}Cl]$ (**8**) is obtained. However, iridium precursor with these ligands yielded neutral bidentate complexes (**3**, **6** and **9**) having the general formula $[Cp^*Ir\{\kappa^2_{(NN')}L\}Cl]$ where L = L1, L2 and L3 respectively. Some of these complexes have been treated with sodium azide to yield azido compounds. Conformational switching of the benzothiazole hydrazone derivatives of complexes **2** and **5** from trans (*E*) to cis (*Z*) are observed on treatment with sodium azide. These azido complexes obtained, have been treated with activated acetylenes of dimethyl and diethyl acetylene carboxylates, which undergo [3 + 2] cycloadditions to form arene ruthenium triazolato complexes. All these complexes have been characterized by analytical, spectroscopic and single crystal x-ray diffraction studies. These complexes have also been carried out for antibacterial studies, but unfortunately none of these compounds or ligands exhibits antibacterial activity towards gram-positive and gram-negative bacteria.

1. Introduction

Half-sandwich complexes of some platinum group metals (ruthenium, rhodium and iridium) have occupied a significant position in organometallic chemistry due to their readiness to form stable complexes with a variety of ligands [1,2]. The dimeric chloro bridged complexes $[\{(arene)M(\mu\text{-}Cl)Cl\}_2]$ where arene = benzene, p-cymene, hexamethylbenzene and M = Ru and $[\{Cp^*M(\mu\text{-}Cl)Cl\}_2]$ where M = Rh or Ir have been the subject of exploration by many research groups as they are useful starting materials [3]. These half sandwich complexes have unique properties; the mild reaction conditions required for synthesis, high yields and a wide range of stability under aqueous conditions have enabled them to occupy a respectable position in organometallic chemistry. Their complexes have found application as good catalysts in water oxidation [4], hydrogen activation [5], transfer hydrogenation [6] and aerobic alcohol oxidation [7]. In addition, their complexes are also found to be biologically active against cancer and bacteria [8].

Vast number of researchers has paid considerable interest in the development of new compounds with activities such as anticancer, anti-malarial, antimicrobial *etc.* Hydrazones derivative constitute an important class of compounds for development of such new drugs. Therefore, many researchers have synthesized a variety of these compounds as target structures and evaluated their biological activities. Although benzothiazole hydrazones itself displayed wide range of biological activities yet only few reports on the chemistry of ruthenium, rhodium and iridium complexes containing these hydrazone derivatives. Souvik and co-worker [9] have studied the

* Corresponding author.
E-mail address: mohanrao59@gmail.com (M.R. Kollipara).

https://doi.org/10.1016/j.jorganchem.2019.04.007
0022-328X/

antimalarial activity of these related benzothiazole hydrazones. Priyanka and co-worker [10] have developed a series of novel 2-substituted hydrazino-6-fluoro-1,3-benzothiazole derivatives that show antimicrobial activity. Felipe and co-worker [11] reported that these small benzothiazole molecule were able to induce apoptosis and prevent metastasis through DNA interaction and *c-MYC* gene suppression in diffuse-type gastric adenocarcinoma cell line. Hence, the choice of ligand plays a crucial role in determining the application of these complexes. Hydrazone functional group in addition to its biological application, displayed interesting structural properties. The presence of nucleophilic imine and amino type nitrogen's, an imine carbon that has both electrophilic and nucleophilic character, configurational isomerism of the C=N group and in most cases an acidic N–H proton enables them to display varieties of bonding with other metals [12].

Keeping in mind the biological activity of benzothiazole hydrazone derivatives we are interested to explore this possibility and also to study the reactivity of *p*-cymene ruthenium and Cp* rhodium complexes containing these derivatives towards NaN_3 and with acetylene carboxylates {dimethylacetylenedicarboxylate (DMAD) and diethylacetylenedicarboxylate (DEAD)}. These azido and triazole compounds containing arene ruthenium complexes have been reported by our group in recent publications [13,14] mainly for neutral complexes. With an objective to promote the applications of platinum group hydrazone complexes bearing benzothiazole hydrazone derivatives, we herein report the synthesis, reactivity, spectral characterization and structural studies of arene ruthenium, rhodium and iridium complexes containing benzothiazole hydrazone ligands L1, L2 and L3 (Chart 1). Antibacterial studies for all the compounds have been carried out but none of them show any significant inhibition towards gram-positive and gram-negative bacteria (experimental details and results has been presented in supplementary material). The molecular structures of representative complexes were determined by single crystal X-ray diffraction.

2. Experimental

2.1. Material and methods

All the reagents were purchased from commercial sources and used as received. Benzaldehyde, *p*-tolualdehyde, *p*-fluorobenzaldehyde was obtained from Merck and 2-hydrazino-benzaldehyde from Alfa Aesar. The solvents were purified and dried according to standard procedures. Precursor of rhodium and iridium $[Cp^*Rh/IrCl_2]_2$ were prepared by a new procedure using Anton Par Monowave 50. Ligands L1, L2 and L3 have been prepared according to the reported procedure [15]. Infrared spectra were recorded on a Perkin-Elmer 983 spectrophotometer by using KBr pellets in the range of 400–4000 cm^{-1}. ^1H NMR spectra were recorded on a Bruker Avance II 400 MHz spectrometer using DMSO-d_6 and $CDCl_3$ as solvents. Absorption spectra were recorded on a Perkin-Elmer Lambda 25 UV/Visible spectrophotometer in the range of 200–800 nm at room temperature in acetonitrile. Mass spectra were recorded using HRMS model Xevo XS QT of mass spectrometer, Waters ACQUITY UHPLC and Waters ZQ 4000 MS instrument by ESI method using acetonitrile as solvent. Elemental analyses of the complexes were performed on a Perkin-Elmer 2400 CHN/S analyzer. All these mononuclear metal complexes were synthesized and characterized by using FT-IR, ^1H NMR, UV–Vis and Single-crystal X-ray diffraction techniques.

2.2. Single-crystal X-ray structures analyses

Single crystal X-ray diffraction data for some of the complexes were collected on an Oxford Diffraction Xcalibur Eos Gemini diffractometer at 293 K using graphite monochromated Mo-Kα radiation ($\lambda = 0.71073$ Å). Suitable crystals were selected and each mounted on a glass fiber. The strategy for the data collection was evaluated using the CrysAlisPro CCD software [16]. Crystal data were collected by standard "phi–omega scan" techniques and were scaled and reduced using CrysAlisPro RED software. Using Olex2 [17] the structures were solved with ShelXT [18] solution program using direct method and refined with olex2.refine [19] refinement package using Gauss-Newton minimization. Crystallographic and structure refinement details for the complexes are summarized in Table S1 and selected bond lengths and bond angles are presented in Table 1. Figs. 1–4 were drawn with ORTEP3 program [20].

2.3. New procedure for synthesis of rhodium and iridium dimer

In a sample test tube of size 10 ml 500 mg of $Rh/IrCl_3.nH_2O$, 0.4 ml of Cp* and 2 ml of dry methanol was added and mix thoroughly. A small size Teflon coated magnetic stirrer was inserted for stirring purpose. The mixture was sealed tightly and placed into an Anton Paar Mono-Wave 50 instrument. The reaction condition was adjusted by setting the temperature to 110 °C and pressure will reach around 20 bars for 45 min. The instrument takes about 2–3 min to heat up to the set temperature and the reaction proceeds smoothly for 45 min. On completion, the reaction cools down to a temperature of 60 °C. A red-orange crystalline solid was obtained. The solvent was decanted, washed several times with diethyl ether and dry in vacuum.

Yield: 87% for Rhodium dimer and 90% for Iridium dimer.

2.4. General procedure for synthesis of cationic and neutral complexes (1–9)

A mixture of starting metal precursor (0.05 mmol) and appropriate ligand (**L**) (0.1 mmol) were dissolved in dry methanol (10 ml) and stirred at room temperature for 8 h (Scheme 1). The solvent was evaporated using rotavapor, the residue was dissolved in

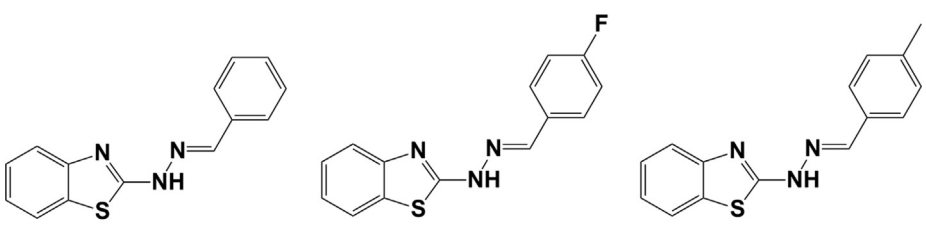

L1 L2 L3

Chart 1. Ligand used in this study.

Table 1
Crystal structure data and refinement of complexes **2**, **3**, **4**, **5**, **6** and **11**.

Complexes	[**2**]	[**3**]	[**4**]	[**5**]	[**6**]	[**11**]
Empirical formula	$C_{24}H_{26}Cl_2N_3SRh$	$C_{24}H_{25}ClN_3SIr$, CH_2Cl_2	$C_{24}H_{23}ClFN_3SRu$	$C_{24}H_{25}Cl_2FN_3SRh$	$C_{24}H_{24}ClFN_3SIr$	$C_{48}H_{50}Cl_{0.60}N_{10.20}Rh_2S_2$
Formula weight	562.37	700.15	541.05	580.01	633.21	1060.95
Temperature (K)	292.9(2)	292.66(10)	292.8(2)	291.8(5)	292.4(3)	293(2)
Wavelength (Å)	0.71073	0.71073	0.71073	0.71073	0.71073	0.71073
Crystal system	monoclinic	monoclinic	monoclinic	monoclinic	monoclinic	monoclinic
Space group	$P2_1/n$	$P2_1/c$	$P2_1/c$	$P21/n$	$P2_1/n$	$P2_1/n$
a (Å)/α (°)	14.4345(7)/90	14.4448(6)/90	17.7740(9)/90	14.4940(8)/90	8.8969(5)/90	26.446(3)/90
b (Å)/β (°)	8.4524(4)/92.641(4)	8.1096(2)/90.618(5)	7.7199(4)/106.497(5)	8.5073(6)/92.789(5)	20.003(13)/93.567(5)	7.4501(4)/118.774(12)
c (Å)/γ (°)	19.7874(11)/90	22.4476(12)/90	16.7258(9)/90	19.6503(9)/90	13.2810(9)/90	26.807(2)/90
Volume ($Å^3$)	2411.6(2)	1260.1(5)	2200.5(2)	2420.1(3)	2359.0(2)	4629.5(8)
Z	4	4	4	4	4	4
Density (calc) (Mg/m^{-3})	1.5488	1.7686	1.6330	1.5918	1.7828	1.522
Absorption coefficient	1.033	5.481	0.954	1.038	5.886	0.884
F(000)	1141.5	1365.6	1092.5	1172.2	1228.5	2166
Crystal size (mm^3)	0.12 × 0.09 x 0.06	0.25 × 0.23 x 0.21	0.25 × 0.23 x0.21	0.25 × 0.23 x 0.21	0.25 × 0.21 x 0.11	0.25 × 0.23 x 0.11
Theta range for data collection	6.92–52.74°	6.68–52.74°.	6.6–52.74°	6.7–52.74°	6.48–52.74°	3.120–25.349°
Index ranges	−12 ≤ h<=19, −11 ≤ k<=10, −22 ≤ l<=25	−19 ≤ h<=19, −10 ≤ k<=9, −29 ≤ l<=19	−24 ≤ h<=12, −10 ≤ k<=10, −22 ≤ l < 21	−16 ≤ h<=18, −11 ≤ k<=11, −26 ≤ l < 15	−8 ≤ h<=12, −23 ≤ k<=26, −16 ≤ l < 17	−31 ≤ h<=17, −8 ≤ k<=8, −27 ≤ l < 32
Reflections collected	9312	11076	9340	9993	10241	15966
Independent reflections	4892 [R_{int} = 0.0397]	5334 [R_{int} = 0.0369]	4486 [R_{int} = 0.0346]	4919 [R_{int} = 0.0276]	4790 [R_{int} = 0.0290]	8432 [R_{int} = 0.0764]
Completeness to theta = 25.00°	98.78%	99.4%	99.5%	99.4%	99.2%	99.7%
Absorption correction	Semi-empirical from equivalents	Semi-empirical from equivalents	Semi-empirical from equivalents	Semi-empirical from equivalents	Semi-empirical from equivalents	Semi-empirical from equivalents
Refinement method	Full-matrix least-squares on F2	Full-matrix least-squares on F2	Full-matrix least-squares on F2	Full-matrix least-squares on F2	Full-matrix least-squares on F2	Full-matrix least-squares on F2
Data/restraints/parameters	4892/0/285	5334/0/303	4486/0/283	4919/0/295	4790/0/285	8432/142/571
Goodness-of-fit on F_2	0.963	1.052	0.995	1.046	1.057	1.214
Final R indices [I > 2sigma(I)]	R1 = 0.0427, wR2 = 0.0710	R1 = 0.0431, wR2 = 0.0851	R1 = 0.0413, wR2 = 0.0766	R1 = 0.0386, wR2 = 0.0798	R1 = 0.0363, wR2 = 0.0629	R1 = 0.1204, wR2 = 0.2010
R indices (all data)	R1 = 0.0696, wR2 = 0.0778	R1 = 0.0592, wR2 = 0.0930	R1 = 0.0665, wR2 = 0.0859	R1 = 0.0544, wR2 = 0.0869	R1 = 0.0519, wR2 = 0.0675	R1 = 0.1561, wR2 = 0.2192
Largest diff. peak and hole ($e.Å^{-3}$)	0.80 and −0.76	1.97 and −1.97	0.87 and −0.75	0.65 and −0.70	1.45 and −1.90	1.237 and −1.339
CCDC No.	1884575	1884576	1884577	1884578	1884579	1884580

Structures were refined on F_0^2: $wR_2 = [\Sigma[w(F_0^2 - F_c^2)^2]/\Sigma w(F_0^2)^2]^{1/2}$, where $w^{-1} = [\Sigma(F_0^2)+(aP)^2+bP]$ and $P = [\max(F_0^2, 0) + 2F_c^2]/3$.

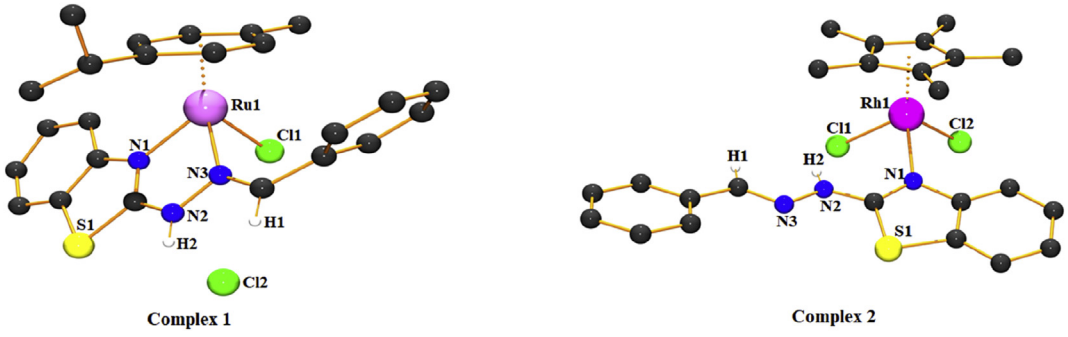

Fig. 1. ORTEP generated molecular structure of complexes **1** and **2** with 50% thermal ellipsoid probability. Because of low theta value, the crystal structure of complex **1** is presented just to show its solid-state composition.

dichloromethane and filtered through Celite, the filtrate was concentrated to 1 ml and excess diethyl ether was added to precipitate the compound. The precipitate was collected and dried in vacuum.

*2.4.1. [(p-cymene)Ru(κ^2-(N,N')-L1)Cl]Cl (**1**)*

Yield: 82%, Color: Orange; IR (KBr, cm^{-1}): 3412 $\nu_{(N-H)}$, 3054 $\nu_{(C-H)}$ (sp^2), 1596-1561 $\nu_{(C=N)}$, 1509-1449 $\nu_{(C=C)}$, 759 $\nu_{(C-S)}$. ^1H NMR (400 MHz, Chloroform-*d*) δ 8.76 (s, 1H), 8.14 (d, *J* = 8 Hz, 2H), 7.63–7.42 (m, 6H), 7.23 (t, *J* = 8 Hz, 1H), 5.46 (s, 2H), 5.26 (d, *J* = 8 Hz, 1H), 4.74 (s, 1H), 4.49 (d, *J* = 8 Hz, 1H), 2.46 (sept, 1H), 2.22 (s, 3H), 1.04 (d, *J* = 8 Hz, 3H), 0.87 (d, *J* = 4 Hz, 3H). ESI-MS (*m*/*z*): 524.02 $[M-Cl]^+$, 488.05 $[M-Cl_2]^+$; UV–Vis {Acetonitrile, λ_{max} nm ($\varepsilon/10^{-4}\,M^{-1}\,cm^{-1}$)}: 212 (7.275), 297 (2.340), 340 (2.174), 386

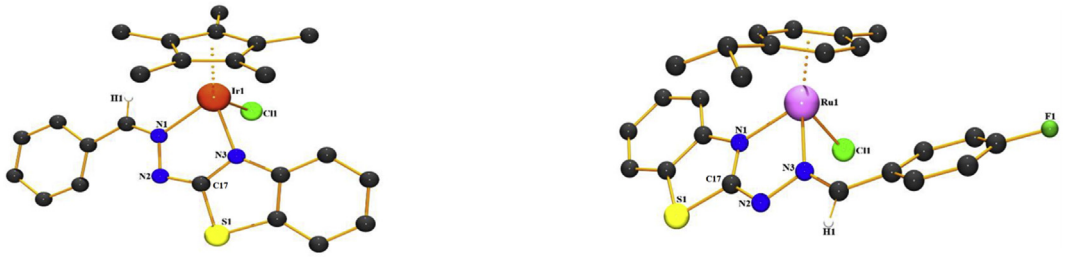

Fig. 2. ORTEP generated molecular structure of complexes **3** and **4** with 50% thermal ellipsoid probability.

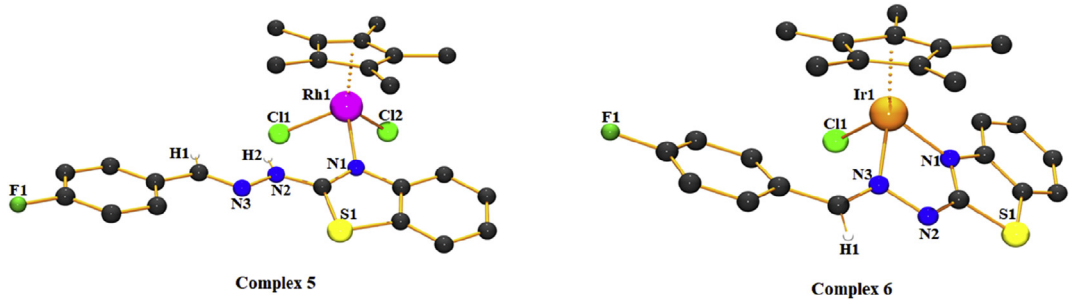

Fig. 3. ORTEP generated molecular structure of complexes **5** and **6** with 50% thermal ellipsoid probability.

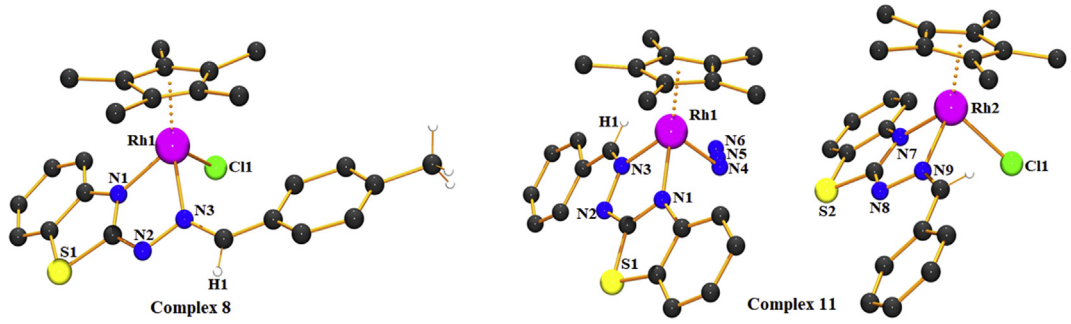

Fig. 4. ORTEP generated molecular structure of complexes **8** and **11** with 50% thermal ellipsoid probability. Complex **11** shows interesting chemical disorder with one set containing two azides, the other an azide group and a chloride group. Because of low theta value, the crystal structure of complexes **8** is presented just to show its solid-state composition.

(1.697).

*2.4.2. [Cp*Rh($\kappa^1_{(N)}$-L1)Cl] (**2**)*

Yield: 85%, Color: Orange; IR (KBr, cm^{-1}): 3060 $\nu_{(C-H)}$ (sp^2), 1602-1560 $\nu_{(C=N)}$, 1489-1452 $\nu_{(C=C)}$, 759 $\nu_{(C-S)}$. ^1H NMR (400 MHz, DMSO-d_6) δ 8.08 (s, 1H), 7.69 (d, $J = 8$ Hz, 2H), 7.63 (d, $J = 4$ Hz, 1H), 7.59–7.54 (m, 1H), 7.49 (d, $J = 8$ Hz, 1H), 7.39 (m, 3H), 7.28 (t, $J = 8$ Hz, 1H), 7.10 (t, $J = 8$ Hz, 1H), 1.75 (s, 15H). UV–Vis {Acetonitrile, λ_{max} nm ($\varepsilon/10^{-4}\,M^{-1}\,cm^{-1}$)}: 225 (8.803), 333 (7.641), 395 (0.891).

*2.4.3. [Cp*Ir($\kappa^2_{(NN')}$-L1)Cl] (**3**)*

Yield: 83%, Color: Yellow; IR (KBr, cm^{-1}): 3060 $\nu_{(C-H)}$ (sp^2), 1599-1561 $\nu_{(C=N)}$, 1489-1453 $\nu_{(C=C)}$, 759 $\nu_{(C-S)}$. ^1H NMR (400 MHz, chloroform-*d*) δ 7.96 (s, 1H), 7.60 (d, $J = 8$ Hz, 3H), 7.44 (d, $J = 8$ Hz, 1H), 7.36–7.19 (m, 5H), 7.04 (t, $J = 8$ Hz, 1H), 1.67 (s, 15H). ESI-MS (*m*/*z*): 616.18 $[M]^+$, 580.16 $[M\text{-}Cl]^+$; UV–Vis {Acetonitrile, λ_{max} nm ($\varepsilon/10^{-4}\,M^{-1}\,cm^{-1}$)}: 222 (6.101), 332 (5.555), 403 (0.443).

*2.4.4. [(p-cymene)Ru($\kappa^2_{(NN')}$-L2)Cl] (**4**)*

Yield: 87%, Color: Yellow; IR (KBr, cm^{-1}): 3060 $\nu_{(C-H)}$ (sp^2), 1601-1562 $\nu_{(C=N)}$, 1506-1452 $\nu_{(C=C)}$, 754 $\nu_{(C-S)}$. ^1H NMR (400 MHz, Chloroform-*d*) δ 8.76 (s, 1H), 8.26 (dd, $J = 8$ Hz, 4 Hz, 2H), 7.63 (d, $J = 8$ Hz, 1H), 7.52–7.44 (m, 2H), 7.25 (m, 3H), 5.46 (s, 2H), 5.32 (d, $J = 4$ Hz, 1H), 4.61 (d, $J = 8$ Hz, 1H), 2.55–2.45 (sept, 1H), 2.24 (s, 3H), 1.07 (d, $J = 8$ Hz, 3H), 0.88 (d, $J = 8$ Hz, 3H). ESI-MS (*m*/*z*): 542.01 $[M\text{-}Cl]^+$, 506.04 $[M\text{-}Cl_2]^+$; UV–Vis {Acetonitrile, λ_{max} nm ($\varepsilon/10^{-4}\,M^{-1}\,cm^{-1}$)}: 213 (7.908), 273 (2.598), 302 (2.593), 336 (2.638).

*2.4.5. [Cp*Rh($\kappa^1_{(N)}$-L2)Cl_2] (**5**)*

Yield: 85%, Color: Orange; IR (KBr, cm^{-1}): 3432 $\nu_{(N-H)}$, 3032 $\nu_{(C-H)}$ (sp^2), 1601-1562 $\nu_{(C=N)}$, 1507-1452 $\nu_{(C=C)}$, 757 $\nu_{(C-S)}$. ^1H NMR (400 MHz, DMSO-d_6) δ 8.00 (s, 1H), 7.62 (d, $J = 8$ Hz, 2H), 7.54 (d, 1H), 7.34–7.28 (m, 3H), 7.22 (t, $J = 8$ Hz, 1H), 7.04 (t, $J = 8$ Hz, 1H), 1.66 (s, 15H); UV–Vis {Acetonitrile, λ_{max} nm ($\varepsilon/10^{-4}\,M^{-1}\,cm^{-1}$)}: 223 (6.892), 331 (5.118), 392 (0.988).

*2.4.6. [Cp*Ir($\kappa^2_{(NN')}$-L2)Cl_2] (**6**)*

Yield: 82%, Color: Yellow; IR (KBr, cm^{-1}): 3430 $\nu_{(N-H)}$, 3054 $\nu_{(C-H)}$ (sp^2), 1601-1563 $\nu_{(C=N)}$, 1508-1453 $\nu_{(C=C)}$, 756 $\nu_{(C-S)}$. ^1H NMR (400 MHz, DMSO-d_6) δ 8.09 (s, 1H), 7.73–7.66 (m, 3H), 7.41 (d, $J = 4$ Hz, 1H), 7.25 (t, $J = 8$ Hz, 1H), 7.18 (t, $J = 8$ Hz, 2H), 7.07 (t, $J = 8$ Hz, 1H), δ 1.65 (s, 15H); ESI-MS (*m*/*z*): 598.14 $[M\text{-}Cl_2]^+$; UV–Vis {Acetonitrile, λ_{max} nm ($\varepsilon/10^{-4}\,M^{-1}\,cm^{-1}$)}: 220 (7.904), 239 (5.585), 332 (7.090) 399 (0.296).

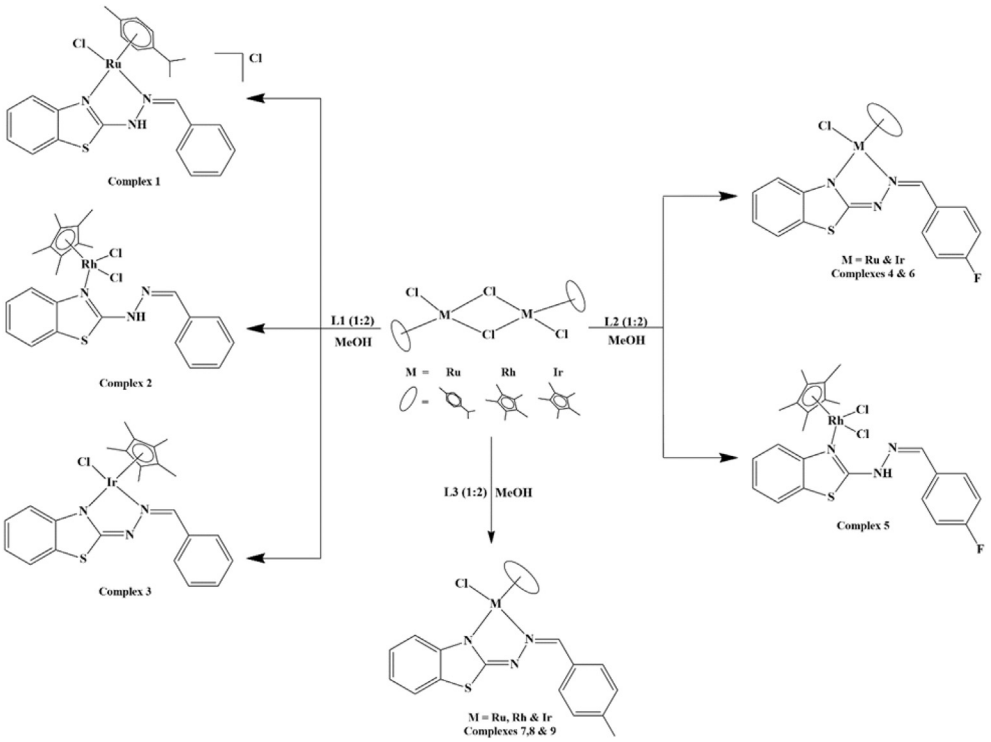

Scheme 1. Schematic representation for the synthesis of complexes **1**–**9**.

*2.4.7. [(p-cymene)Ru($\kappa^2_{(NN')}$-L3)Cl] (**7**)*

Yield: 84%, Color: Yellow; IR (KBr, cm^{-1}): 3430 $\nu_{(N-H)}$, 3054 $\nu_{(C-H)}$ (sp^2), 1601-1563 $\nu_{(C=N)}$, 1508-1453 $\nu_{(C=C)}$, 756 $\nu_{(C-S)}$. ^{1}H NMR (400 MHz, Chloroform-*d*) δ 8.78 (s, 1H), 8.13 (d, J = 8 Hz, 2H), 7.68 (d, J = 8 Hz, 1H), 7.69–7.51 (m, 2H), 7.39 (d, J = 8 Hz, 2H), 7.32 (t, J = 8 Hz, 1H), 5.52 (d, J = 4 Hz, 2H), 5.31 (d, J = 8 Hz, 1H), 4.71 (d, J = 4 Hz, 1H), 2.59–2.50 (m, 4H), 2.33 (s, 3H), 1.13 (d, J = 8 Hz, 3H), 0.97 (d, J = 8 Hz, 3H). UV–Vis {Acetonitrile, λ_{max} nm ($\varepsilon/10^{-4}\,M^{-1}\,cm^{-1}$)}: 211 (9.537), 267 (3.779) 299 (3.435) 351 (3.322) 393 (2.975).

*2.4.8. [Cp*Rh($\kappa^2_{(NN')}$-L3)Cl_2] (**8**)*

Yield: 83%, Color: Orange; IR (KBr, cm^{-1}): 3432 $\nu_{(N-H)}$, 3032 $\nu_{(C-H)}$ (sp^2), 1601-1562 $\nu_{(C=N)}$, 1507-1452 $\nu_{(C=C)}$, 757 $\nu_{(C-S)}$. ^{1}H NMR (400 MHz, DMSO-d_6) 8.08 (s, 1H), 7.74 (d, J = 4 Hz, 1H), 7.57 (d, J = 8 Hz, 2H), 7.42 (s, 1H), 7.29–7.24 (m, 3H), 7.09 (t, J = 8 Hz, 1H), 2.33 (s, 3H), 1.61 (s, 15H); UV–Vis {Acetonitrile, λ_{max} nm ($\varepsilon/10^{-4}\,M^{-1}\,cm^{-1}$)}: 225 (8.228), 243 (5.849), 333 (7.0002), 391 (0.958).

*2.4.9. [Cp*Ir($\kappa^2_{(NN')}$-L3)Cl] (**9**)*

Yield: 81%, Color: Yellow; IR (KBr, cm^{-1}): 3430 $\nu_{(N-H)}$, 3054 $\nu_{(C-H)}$ (sp^2), 1601-1563 $\nu_{(C=N)}$, 1508-1453 $\nu_{(C=C)}$, 756 $\nu_{(C-S)}$. ^{1}H NMR (400 MHz, DMSO-d_6) δ 8.08 (s, 1H), 7.75 (d, J = 4 Hz, 1H), 7.57 (d, J = 8 Hz, 2H), 7.42 (s, 1H), 7.29–7.24 (m, 3H), 7.09 (t, J = 8 Hz, 1H), 2.32 (s, 3H), 1.61 (s, 15H); ESI-MS (m/z): 598.14 $[M\text{-}Cl_2]^+$; UV–Vis {Acetonitrile, λ_{max} nm ($\varepsilon/10^{-4}\,M^{-1}\,cm^{-1}$)}: 221 (8.614), 244 (5.953), 333 (8.555), 398 (0.712).

*2.5. General procedure for synthesis of azido complexes (**10**–**15**)*

The corresponding starting complexes of **1**, **2**, **4**, **6**, **7, 8** and NaN_3 in 1:4 M ratio was suspended in dry methanol (15 ml) and stirred at room temperature for 6 h (Scheme 2). The solvent was removed to dryness using rotary evaporator. The residue was extracted with dichloromethane, filtered and precipitated with hexane.

*2.5.1. [(p-cymene) Ru($\kappa^2_{(NN')}$-L1)N_3] (**10**)*

Yield: 68%, Color: Yellow; IR (KBr, cm^{-1}): 3058 $\nu_{(C-H)}$ (sp^2), 2026 $\nu_{(N3)}$, 1634-1577 $\nu_{(C=N)}$, 1484-1450 $\nu_{(C=C)}$, 748 $\nu_{(C-S)}$. ^{1}H NMR (400 MHz, Chloroform-*d*) δ 8.30 (d, J = 8 Hz, 2H), 8.00 (s, 1H), 7.49–7.44 (m, 3H), 7.42 (d, J = 4 Hz, 1H), 7.36 (d, J = 8 Hz, 2H), 7.04 (t, J = 4 Hz, 1H), 5.79 (d, J = 4 Hz, 1H), 5.65 (d, J = 8 Hz, 1H), 5.54 (d, J = 4 Hz, 1H), 5.29 (d, J = 8 Hz, 1H), 2.49 (sept, 1H), 2.33 (s, 3H), 1.09 (d, J = 8 Hz, 3H), 1.02 (d, J = 8 Hz, 3H).

*2.5.2. [Cp*Rh($\kappa^2_{(NN')}$-L1)N_3] (**11**)*

Yield: 75%, Color: Orange; IR (KBr, cm^{-1}): 3060 $\nu_{(C-H)}$(sp^2), 2019 $\nu_{(N3)}$, 1635 $\nu_{(C=N)}$, 1497-1450 $\nu_{(C=C)}$, 782 $\nu_{(C-S)}$. ^{1}H NMR (400 MHz, chloroform-*d*) δ 8.76 (s, 1H), 8.09 (d, J = 8 Hz, 2H), 7.49 (t, J = 8 Hz, 2H), 7.43 (t, J = 8 Hz, 2H), 7.27–7.19 (m, 2H), 6.96 (t, J = 8 Hz, 1H), 1.39 (s, 15H).

*2.5.3. [(p-cymene)Ru($\kappa^2_{(NN')}$-L2)N_3] (**12**)*

Yield: 71%, Color: Orange; IR (KBr, cm^{-1}): 3060 $\nu_{(C-H)}$ (sp^2), 2027 $\nu_{(N3)}$, 1645-1597 $\nu_{(C=N)}$, 1488-1452 $\nu_{(C=C)}$, 748 $\nu_{(C-S)}$. ^{1}H NMR (400 MHz, Chloroform-*d*) δ 8.72 (s, 1H), 8.18 (dd, J = 4 Hz, 4 Hz, 2H), 7.43 (d, J = 8 Hz, 1H), 7.29–7.20 (m, 4H), 6.99 (t, J = 8 Hz, 1H), 5.54 (d, J = 8 Hz, 1H), 5.37 (d, J = 4 Hz, 1H), 5.03 (d, J = 4 Hz, 1H), 4.50 (d, J = 4 Hz, 1H), 2.43–2.30 (m, 4H), 1.08 (d, J = 4 Hz, 3H), 0.99 (d, J = 8 Hz, 3H).

*2.5.4. [Cp*Rh($\kappa^2_{(NN')}$-L2)N_3] (**13**)*

Yield: 68.3%, Color: Orange.; IR (KBr, cm^{-1}): 3032 $\nu_{(C-H)}$ (sp^2), 2019 $\nu_{(N3)}$, 1635-1562 $\nu_{(C=N)}$, 1497-1450 $\nu_{(C=C)}$, 758 $\nu_{(C-S)}$. ^{1}H NMR (400 MHz, Chloroform-*d*) δ 8.79 (s, 1H), 8.13 (dd, J = 8 Hz, 8 Hz, 2H), 8.04 (d, J = 8 Hz, 1H), 7.52 (d, J = 4 Hz, 1H), 7.20 (t, J = 8 Hz, 3H), 6.97 (t, J = 8 Hz, 1H), 1.47 (s, 15H).

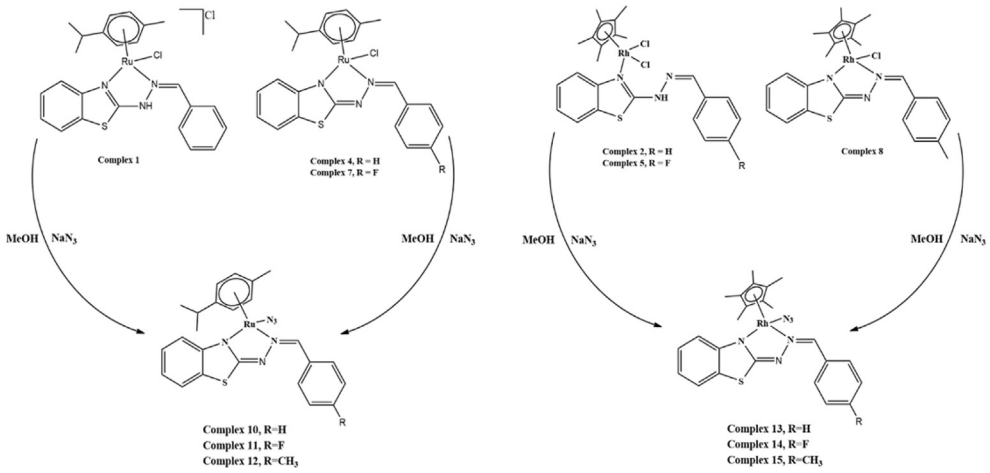

Scheme 2. Schematic representations for the synthesis of azido complexes **10**–**15**.

*2.5.5. [(p-cymene)Ru($\kappa^2_{(NN')}$-L3)N_3] (**14**)*

Yield: 72%, Color: Red.; IR (KBr, cm^{-1}): 3058 $\nu_{(C-H)}$ (sp^2), 2020 $\nu_{(N3)}$, 1644-1575 $\nu_{(C=N)}$, 1491-1451 $\nu_{(C=C)}$, 746 $\nu_{(C-S)}$. ^{1}H NMR (400 MHz, Chloroform-*d*) δ 8.20 (d, *J* = 8 Hz, 2H), 7.97 (s, 1H), 7.47 (d, *J* = 8 Hz, 1H), 7.30–7.23 (m, 4H), 7.03 (dt, *J* = 4 Hz, 4 Hz, 1H), 5.77 (d, *J* = 8 Hz, 1H), 5.64 (d, *J* = 8 Hz, 1H), 5.53 (d, *J* = 8 Hz, 1H), 5.28 (d, *J* = 8 Hz, 1H), 2.54–2.41 (m, 4H), 2.33 (s, 3H), 1.09 (d, *J* = 8 Hz, 3H), 1.02 (d, *J* = 4 Hz, 3H).

*2.5.6. [Cp*Rh($\kappa^2_{(NN')}$-L3)N_3] (**15**)*

Yield: 69%, Color: Orange; IR (KBr, cm^{-1}): 3032 $\nu_{(C-H)}$ (sp^2), 2021 $\nu_{(N3)}$, 1634-1571 $\nu_{(C=N)}$, 1497-1454 $\nu_{(C=C)}$, 757 $\nu_{(C-S)}$. ^{1}H NMR (400 MHz, Chloroform-*d*) δ 8.72 (s, 1H), 7.98 (d, *J* = 8 Hz, 2H), 7.41 (d, *J* = 8 Hz, 1H), 7.31–7.18 (m, 4H), 6.95 (t, *J* = 8 Hz, 1H), 2.44 (s, 3H), 1.41 (s, 15H).

*2.6. Reactivity studies of azido complexes with acetylenes (**16**–**21**)*

Into a round bottom flask, charged with the corresponding azido complexes **10**–**15**, excess of dimethylacetylene dicarboxylate/ diethylacetylene dicarboxylate and dichloromethane (20 ml) was added. The mixture was stirred at room temperature for 16 h (Scheme 3). The solution was evaporated to 2 ml on a water bath. To this solution, 30 ml of hexane was added whereby the compound precipitated out as a yellow solid. The solid was washed with hexane (2 × 20 ml), collected and dried in vacuum.

*2.6.1. [(p-cymene)Ru($\kappa^2_{(NN')}$-L1){$N_3C_2(CO_2Me)_2$}] (**16**)*

Yield: 75%; Color: Yellow; FT-IR (KBr, cm^{-1}): 3058 $\nu_{(C-H)}$ (sp^2), 1731 $\nu_{(C=O)}$, 1643 $\nu_{(C=N)}$, 1480-1451 $\nu_{(C=C)}$, 751 $\nu_{(C-S)}$. ^{1}H NMR (400 MHz, Chloroform-*d*) δ 8.34 (s, 1H), 8.30 (d, *J* = 8 Hz, 2H), 7.56 (d, *J* = 8 Hz, 1H), 7.46–7.41 (m, 3H), 7.35 (tt, *J* = 8 Hz, 4 Hz, 2H), 7.04 (t, *J* = 8 Hz, 1H), 5.90 (d, *J* = 4 Hz, 1H), 5.81 (d, *J* = 8 Hz, 1H), 5.76 (d, *J* = 8 Hz, 1H), 5.56 (d, *J* = 8 Hz, 1H), 3.74 (s, 6H), 2.44 (sept, 1H), 1.90 (s, 3H), 1.06 (d, *J* = 8 Hz, 3H), 0.99 (d, *J* = 8 Hz, 3H).

*2.6.2. [(p-cymene)Ru($\kappa^2_{(NN')}$-L1){$N_3C_2(CO_2Et)_2$}] (**17**)*

Yield: 78%; Color: Yellow; FT-IR (KBr, cm^{-1}): 3055 $\nu_{(C-H)}$ (sp^2), 1723 $\nu_{(C=O)}$, 1644 $\nu_{(C=N)}$, 1490-1451 $\nu_{(C=C)}$, 751 $\nu_{(C-S)}$; ^{1}H NMR (400 MHz, Chloroform-*d*) δ 8.35 (s, 1H), 8.29 (d, *J* = 8 Hz, 2H), 7.44–7.40 (m, 4H), 7.36–7.32 (m, 2H), 7.03 (t, *J* = 8 Hz, 1H), 5.89 (d, *J* = 8 Hz, 1H), 5.80 (d, *J* = 8 Hz, 1H), 5.75 (d, *J* = 4 Hz, 1H), 5.57 (d, *J* = 4 Hz, 1H), 4.20 (q, *J* = 8 Hz, 4H), 2.45 (sept, 1H), 1.92 (s, 3H), 1.20 (t, *J* = 8 Hz, 6H), 1.07 (d, *J* = 8 Hz, 3H), 1.00 (d, *J* = 8 Hz, 3H).

*2.6.3. [(p-cymene)Ru($\kappa^2_{(NN')}$-L2){$N_3C_2(CO_2Me)_2$}] (**18**)*

Yield: 77%; Color: Yellow; FT-IR (KBr, cm^{-1}): 3057 $\nu_{(C-H)}$ (sp^2), 1732 $\nu_{(C=O)}$, 1645 $\nu_{(C=N)}$, 1490-1452 $\nu_{(C=C)}$, 617 $\nu_{(C-S)}$; ^{1}H NMR (400 MHz, Chloroform-*d*) δ 8.29–8.19 (m, 3H), 7.49 (d, *J* = 8 Hz, 1H), 7.38 (d, *J* = 8 Hz, 1H), 7.28 (t, *J* = 8 Hz, 1H), 7.06–6.96 (m, 3H), 5.84 (d, *J* = 4 Hz, 1H), 5.74 (d, *J* = 8 Hz, 1H), 5.69 (d, *J* = 8 Hz, 1H), 5.49 (d, *J* = 8 Hz, 1H), 3.67 (s, 6H), 2.38 (sept, *J* = 6.9 Hz, 1H), 1.83 (s, 3H), 0.99 (d, *J* = 8 Hz, 3H), 0.92 (d, *J* = 8 Hz, 3H).

*2.6.4. [(p-cymene)Ru($\kappa^2_{(NN')}$-L2){$N_3C_2(CO_2Et)_2$}] (**19**)*

Yield: 78%; Color: Yellow; FT-IR (KBr, cm-1): 3055 $\nu_{(C-H)}$ (sp^2), 1732 $\nu_{(C=O)}$, 1643 $\nu_{(C=N)}$, 1491-1450 $\nu_{(C=C)}$, 667 $\nu_{(C-S)}$; ^{1}H NMR (400 MHz, Chloroform-*d*) δ 8.33 (s, 1H), 7.56 (d, *J* = 8 Hz, 1H), 7.48–7.32 (m, 4H), 7.26–7.02 (m, 4H), 5.91 (d, *J* = 4 Hz, 1H), 5.81 (d, *J* = 4 Hz, 1H), 5.77 (d, *J* = 8 Hz, 1H), 5.58 (d, *J* = 8 Hz, 1H), 4.20 (q, *J* = 8 Hz, 4H), 2.45 (sept, 1H), 1.91 (s, 3H), 1.21 (t, *J* = 8 Hz, 6H), 1.06 (d, *J* = 4 Hz, 3H), 0.99 (d, *J* = 8 Hz, 3H). Anal. Calc. for $C_{32}H_{33}FN_6O_4RuS$ (717.78): C, 53.55; H, 4.63; N, 11.71. Found: C, 55.68; H, 4.80; N, 11.87%.

*2.6.5. [(p-cymene)Ru($\kappa^2_{(NN')}$-L3){$N_3C_2(CO_2Me)_2$}] (**20**)*

Yield: 72%; Color: Yellow; FT-IR (KBr, cm-1): 3053 $\nu_{(C-H)}$ (sp^2), 1734 $\nu_{(C=O)}$, 1645 $\nu_{(C=N)}$, 1493-1451 $\nu_{(C=C)}$, 662 $\nu_{(C-S)}$; ^{1}H NMR (400 MHz, Chloroform-*d*) δ 8.24 (s, 1H), 8.13 (d, *J* = 8 Hz, 2H), 7.47 (d, *J* = 8 Hz, 1H), 7.37–7.32 (m, 2H), 7.26 (t, *J* = 8 Hz, 1H), 7.13 (d, *J* = 8 Hz, 1H), 6.95 (t, *J* = 8 Hz, 1H), 5.82 (d, *J* = 4 Hz, 1H), 5.72 (d, *J* = 4 Hz, 1H), 5.67 (d, *J* = 4 Hz, 1H), 5.48 (d, *J* = 8 Hz, 1H), 3.67 (s, 6H), 2.35 (m, 4H), 1.82 (s, 3H), 0.99 (d, *J* = 8 Hz, 3H), 0.92 (d, *J* = 4 Hz, 3H).

*2.6.6. [(p-cymene)Ru($\kappa^2_{(NN')}$-L3){$N_3C_2(CO_2Et)_2$}] (**21**)*

Yield: 75%; Color: Yellow; FT-IR (KBr, cm-1): 3057 $\nu_{(C-H)}$ (sp^2), 1735 $\nu_{(C=O)}$, 1631 $\nu_{(C=N)}$, 1492-1451 $\nu_{(C=C)}$, 619 $\nu_{(C-S)}$; ^{1}H NMR (400 MHz, Chloroform-*d*) δ 8.30 (s, 1H), 8.19 (d, *J* = 8 Hz, 2H), 7.54 (d, *J* = 8 Hz, 1H), 7.41 (t, *J* = 8 Hz, 3H), 7.23 (d, *J* = 8 Hz, 2H), 7.01 (t, *J* = 8 Hz, 1H), 5.87 (d, *J* = 4 Hz, 1H), 5.78 (d, *J* = 8 Hz, 1H), 5.74 (d, *J* = 8 Hz, 1H), 5.55 (d, *J* = 8 Hz, 1H), 4.20 (q, *J* = 8 Hz, 4H), 2.44 (sept, 1H), 2.40 (s, 3H), 1.91 (s, 3H), 1.20 (t, *J* = 8 Hz, 6H), 1.06 (d, *J* = 8 Hz, 3H), 0.99 (d, *J* = 8 Hz, 3H).

3. Results and discussion

3.1. Synthesis of metal complexes

In the present work we have carried out the synthesis and reactivity studies of metal complexes of ruthenium, rhodium and

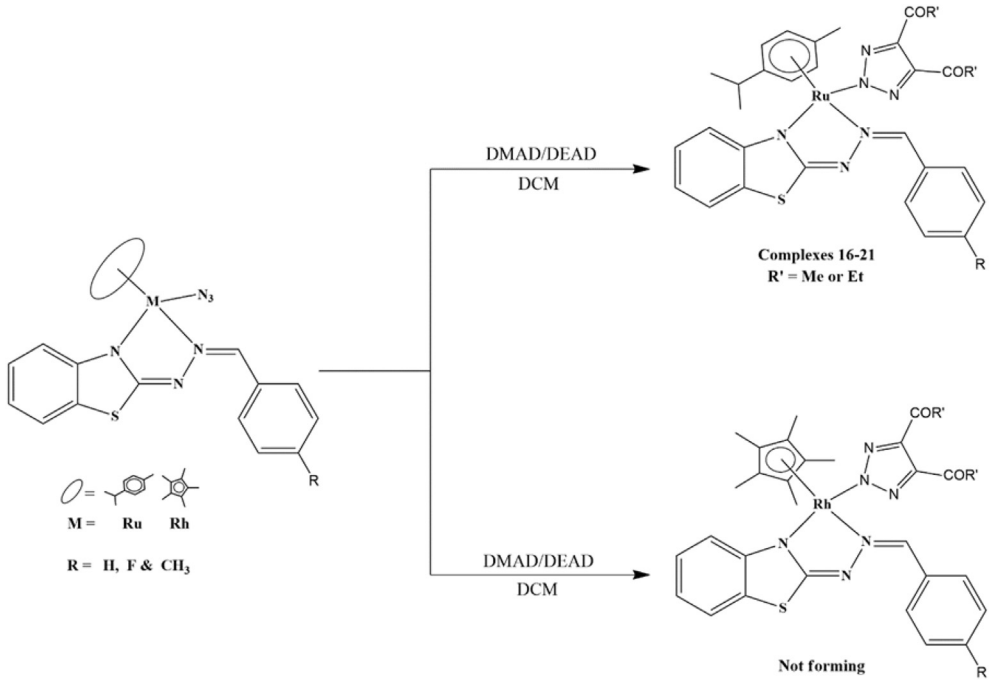

Scheme 3. Schematic representations for the synthesis of triazolato complexes.

iridium containing benzothiazole hydrazone derivatives. Treatment of $[(arene)Ru(\mu\text{-}Cl)Cl]_2$, (arene$_=$ p-cymene), $[Cp^*M(\mu\text{-}Cl)Cl]_2$ (M = Rh and Ir) with ligand (L1, L2 and L3) in 1:2 (M:L) ratio has yielded cationic complexes [(*p*-cymene)Ru(L1)Cl]Cl (**1**) with chloride as counter ion and eight neutral complexes **2**–**9** with different binding mode towards the metal centers. Complexes **1**, **2**, **4**, **5**, **7** and **8** were then treated with sodium azide to yield azido compounds. Cationic complex **1** were able to react with NaN_3 to form neutral azido complex, this is the first time we observed such reaction proceeds where usually the reaction of a cationic complexes with NaN_3 does not occur. This may be attributed due to the presence of an acidic NH proton in the ligand which can deprotonate in solution leading to the formation of neutral bidentate complex. Also monodentate $\kappa^1_{(N)}$ complexes **2** and **5** on reacting with NaN_3 in methanol resulted in the formation of neutral five membered chelated $\kappa^2_{(N,N')}$ azido complexes and a change in conformation of the benzothiazole hydrazone derivatives from *E* to *Z* were observed. These azido compounds were further treated with activated acetylenes of dimethyl and diethyl acetylene carboxylates to yield triazolato complexes. However, triazole compounds of rhodium decompose and could not be separated. All complexes are orange in color except iridium complexes which is yellow in color and triazole complexes which are also yellow in color. These complexes are stable in air as well as in solution. They are soluble in polar organic solvents like dichloromethane, chloroform, acetone and acetonitrile and insoluble in non-polar solvents like hexane, diethyl ether and petroleum ether. The analytical data of these compounds are consistent with the formulations. All complexes are characterized by ^{1}H NMR, IR and Mass spectroscopy. The molecular structure of the complexes determined by single crystal X-ray diffraction method, revealed the different modes of binding of the metals to the ligands L1, L2 and L3 that differs only at para position of the phenyl group.

3.2. Spectral studies of the complexes

3.2.1. IR studies of metal complexes

Complexes **1**–**9** exhibits characteristic stretching frequencies for $\nu_{(N-H)}$, $\nu_{(C=N)}$ and $\nu_{(C-S)}$. The IR spectra of the complexes were compared with that of the free ligand. The free ligands show a characteristic stretching frequency at 3434-3412 cm^{-1} for $\nu_{(N-H)}$ and stretching frequency at 1630 and 1619 cm^{-1} for $\nu_{(C=N)}$. On formation of complexes the C=N stretching frequency decreases and is observed between 1602 and 1561 cm^{-1} and N–H stretching frequency was observed only for complexes **2** and **5** which suggest that coordination occurs only through the benzothiazole nitrogen forming a mono-dentate neutral complexes. The absent of N–H stretching frequency for complexes (**3**, **4**, **6**, **7, 8** and **9**) indicates the formation of bidentate neutral complexes which coordinates through the benzothiazole and imine nitrogen's.

Azido complexes **10**–**15** were confirmed from their IR spectra by the presence of a strong absorption band at around 2018–2027 cm^{-1} which corresponds to terminal ν_{N3}. The formation of triazole complexes **16**–**18** were also confirmed from their IR spectra. The absence of a sharp band at 2018–2017 cm^{-1} and the appearance of a strong band at around 1720-1734 cm^{-1} which corresponds to the stretching frequency of the carbonyl group of esters confirmed the formation of triazole compounds. The IR spectra of some complexes were given in supplementary data (Figure S15 to S18).

3.2.2. ^{1}H NMR studies of the complexes

To further reveal the coordination behavior of the ligands to metal and the formation of triazole complexes, ^{1}H NMR analyses of all these complexes were recorded in deuterated solvent at room temperature. The ligand protons of complex **1** displayed one singlet for NH proton at 4.74 ppm whereas the NH proton signal of complexes **2** and **5,** which were recorded in $CHCl_3$-d_1 and DMSO-d_6 mixture in (3:1) ratio was not observed due to solvent exchange. The disappearance of NH proton signal in complexes **3**, **4**, **6**, **7, 8** and **9** indicates the deprotonation of NH proton of the hydrazine group. The imine proton of all the complexes displayed one singlet at around 7.96–8.76 ppm. Upon co-ordination to the metal center the aromatic proton signals of the ligand are shifted downfield which is due to the donation of lone pairs of electron from the nitrogen atom

of the benzothiazole (N) and the imine nitrogen (N′) to the metal center. In all the complexes several multiplets were observed in the range of 7.44–7.60 ppm due to overlap of the protons of phenyl and benzothiazole rings. All ruthenium complexes (**1**, **4** and **7**) displayed one singlet with two protons at 5.46 ppm and two doublets with one proton each at 5.33–4.48 ppm which corresponds to the aromatic protons of the *p*-cymene ring and the methyl protons of the isopropyl group of the p-cymene ring displayed two doublets in the range of 0.86–1.08 ppm. This unusual splitting of the aromatic and isopropyl protons may be attributed to the diastrophic methyl protons of isopropyl group and chiral nature of the metal center [21,22]. The methine proton of the *p*-cymene ring exhibits a septet in the range of 2.41–2.55 ppm. In addition, complex **7** displayed one singlet at 2.33 ppm for 3 protons of the methyl group in para position of the aldehyde derivative. The methyl singlet of fifteen protons for rhodium and iridium complexes (**2**, **3**, **5**, **6**, **8** and **9**) was observed in the range of 1.65–1.75 ppm. The ^{1}H NMR of all these complexes was given in supplementary data (Figure S1 to S9).

From the ^{1}H NMR spectra of azido complexes **10**–**15**, there is not much different in the splitting pattern of their protons except that their chemical shift value has shifted slightly to the downfield region for all the ruthenium azido complexes. The aromatic protons of the *p*-cymene ring now displayed four doublets in the range of 5.99 to 4.49 ppm instead of one singlet and two doublets, which clearly indicate the formation of different complexes due to the attachment of N3 group to form azido complexes. The diastrophic methyl protons of isopropyl group displayed the same two doublets in the range of 1.30 to 0.98 ppm and the methine protons of the *p*-cymene ring of all the ruthenium azido complexes displayed a septet in the range of 2.74 to 2.34 ppm. In the case of rhodium azido complexes the ligand protons shifted towards the downfield region while the Cp* protons shifted towards the up field region 1.3–1.4 ppm as compared to their relative complexes where the Cp* protons displayed in region of 1.6–1.7 ppm. The deprotonation of NH proton for mono-dentate rhodium complexes **2** and **5** to form bidentate neutral azido complexes **11** and **13** could not be explained from their NMR spectra due to the absence of NH protons signal in the spectra of the former. However, this is being confirmed from their solid-state structure obtained by single crystal X-ray diffraction (SXRD) method, which indicates the formation of azido complexes along with the conversion of mono-dentate to bidentate complexes, which is similar to the complexes reported by our group [12,13].

The ^{1}H NMR of triazolato complexes based from previous reported articles the triazole anion can coordinate to the metal center *via* N(1) or N(2) nitrogen atoms [23,24] forming two types of isomer which are isoenergetic as confirmed by molecular calculation [24,25]. However, these isomers can be easily differentiated from their ^{1}H NMR spectra as they displayed different splitting pattern. Based on the evidence obtained from previous articles, these two isomers can either be formed simultaneously [23–26] or in some cases N(2) bound isomer being formed exclusively [23,26–28]. Both of these evidence were true depending on the overall stability of the complexes either kinetically N(1) and thermodynamically N(2) as our group have reported in previous article [29]. Other factors that determined the formation of N(1) or N(2) bound isomers are electronic factor such as nucleophilicity of the triazole anion which favor N(1) bound isomer or steric factor which arises upon coordination of the ligands to the metal center which favor N(2) bound isomer [30]. In this present work, we obtained exclusively only the N(2) bound isomers for both alkoxy substituted acetylenes. The ^{1}H NMR spectra of triazolato complexes **16**–**21** displayed characteristic peaks corresponding to the ligands (L1, L2 and L3) and the *p*-cymene moiety. In addition, the ^{1}H NMR of complexes **16**, **18** and **20** displayed a singlet in the range of 3.67–3.74 ppm, which corresponds to the six protons of the methoxy carbonyl group. Also, from the ^{1}H NMR of complexes **17**, **19** and **21** the ethoxy carbonyl group displayed a quartet in the range of 4.17–4.23 ppm, which corresponds to the four protons of the methylene group and a triplet in the range of 1.18–1.23 ppm which corresponds to the six protons of the methyl group. These splitting pattern clearly suggest the formation of N(2) bound isomer as reported by our group [13,14,29]. The ^{1}H NMR spectra of some of these triazolato complexes were given in supplementary data (Figure S10 to S14).

3.2.3. Mass studies of the complexes

The mass spectra of some of the complexes **1**, **3** and **4** are presented in supplementary data (Figure S19 to S21). Complex **1** display its predominant molecular ion peak at *m*/*z*: 488.05 which corresponds to $[M\text{-}Cl_2]^+$ ion peak whereas complexes **3** and **4** display their predominant molecular ion peaks at *m*/*z*: 580.16 and *m*/*z*: 506.04 respectively which corresponds to $[M\text{-}Cl]^+$ ion. In cationic complex **1**, fragmentation of the counter ion and the chloride was observed while in neutral complexes **3** and **4** fragmentation of chloride attached to the metal center takes place. The mass spectra values of all these complexes strongly support the formation of the desired product.

3.2.4. UV– visible description of metal complexes

The absorption spectra of ligands and complexes **1**–**9** were recorded in acetonitrile of 10^{-4} M cm^{-1} at room temperature and the UV plot of these complexes along with the ligands is provided in supplementary information Figure S22. The ligand exhibited medium intensity band at 245 nm and a high intensity band at 332 nm corresponding to ligand center π-π* and n-π* transitions [31,32]. An absorption bands in the visible region around 400–450 nm are attributed as charge transfer band. Because of low molar absorptivity values these band maybe assigned as d-d transition.

3.3. Single crystal X-ray structure determination of complexes

Single crystals suitable for X-ray diffraction analysis were obtained for complexes **1**, **2**, **3**, **4**, **5**, **6**, **8** and **11**. These crystals are orange, yellow and red in colors and were obtained by solvent diffusion method for all the complexes except complex **4** which was crystallized from methanol by slow evaporation method. The molecular structures of these complexes have been established by single crystal X-ray structure analysis. Because of low theta value, the molecular structure of complexes **1**, **8** and **11** were given only to confirm their structural composition and binding mode of the ligand towards metal. ORTEP diagrams of these complexes are presented in Figs. 1–4 and their X-ray data collection parameters, selected bond lengths, and selected bond angles are presented in Tables 1 and 2 respectively. Complex **1** crystallize in triclinic with $P\bar{1}$ space group whereas complexes **2**, **5**, **6** and **11** crystallizes in monoclinic with $P2_1/n$ space group and complexes **3** and **4** crystalizes in monoclinic with $P2_1/c$ space group. Complex **8** crystalize in orthorhombic with $Pna2_1$ space group. In complexes **1**, **4** and **7** metal is coordinated to a *p*-cymene and in complexes **2**, **3**, **5**, **6**, **8** and **9** the metal is coordinated to a Cp* ligand as seat. From the molecular structure of complexes the metal (Ru/Rh/Ir) binds to one chloride and two nitrogen donor atoms of the chelating ligand forming half-sandwich three-legged piano stool structure around each metal center. The complexes are mononuclear neutral and cationic only in the case of ruthenium complex **1** in which the ligand with hydrogen (H) substituent at para position of the phenyl ring acts as N∩N donor. However, ruthenium complex **4** with fluorine (F) at para position of the phenyl ring formed neutral bidentate complex (Fig. 2). Complexes of rhodium **2** and **5** with H

and F substituents respectively at para position of the phenyl ring binds to one nitrogen donor atom of the benzothiazole ring and two terminal chlorides forming neutral mono-dentate complexes. The molecular structure of these complexes (Figs. 1 and 3) clearly shows the trans conformation of the benzothiazole hydrazone derivatives. Interestingly when these trans conformers mono coordinated rhodium complexes were treated with sodium azide (chemical activation) [12] in methanol the benzothiazole derivatives undergo conformational switching from trans (*E*) to cis (*Z*) conformers. The formed azido complexes clearly justified the conformational switching of the benzothiazole derivatives as seen from the molecular structure of complex **11** (Fig. 4). This in turn changes the binding modes of the ligands from neutral monodentate to neutral bidentate complexes with the deprotonation of acidic NH proton. Molecular structure of complex **11** shows interesting chemical disorder with one set containing two azides, the other an azide group and a chloride group. In contrast, rhodium complex **8** with methyl group as substituent at para position of the phenyl ring binds to both the nitrogen forming neutral bidentate complex as seen from the molecular structure of the complex (Fig. 4). Hence, the variations in the binding modes of the benzothiazole hydrazone derivatives may also be contributed by the substituents at the para position of the phenyl ring (H, F, CH_3). However, in the case of iridium complexes **3** and **6** (Figs. 2 and 3) the mode of binding of the benzothiazole hydrazone derivatives does not change even when the substituents at para position of the phenyl ring were different. Thus, the variation of bonding of the same ligand towards different metal happen which is not unusual where similar bonding behaviors has been reported by our group with pyridyl azine ligands [33,34].

The distance between the metal center to the centroid of the arene ring in complexes **1**–**6** and **11** are 1.705 Å, 1.773 Å, 1.797 Å, 1.692 Å, 1.769 Å, 1.794 Å and 1.805 Å respectively (Table 2). The M(1)-N(1) bond distances in complexes **1**–**6** and **11** are 2.12(2) Å, 2.167(3) Å, 2.083(5) Å, 2.083(3) Å, 2.161(3) Å, 2.126(4) Å, 2.063(9) Å and M(1)-N(3) bond distances in complexes **1, 3, 4**, **6** and **11** are 2.10(2), 2.113(6), 2.140(3), 2.126(4) and 2.103(8) Å respectively. The M(1)-N(4) bond distance in complex **11** is 2.131(9) Å. The M(1)-Cl(1 or 2) bond distance in these complexes are found to be in the range of 2.3983 Å to 2.4387 Å which is comparable with earlier reported complexes [35,36]. The bond angle values of N(1)-M(1)-(N3) for bidentate complexes are found to be in the range of 75.1°–76.15° and N-M-Cl bond angle values are in the range of 83.1°–92.80° for both mono-dentate and bidentate complexes. The bond angle values of N(1)-M-(N4) and N(3)-M-(N4) in azido complex **11** are in the range of 86.2°–86.5° which is close to that of an octahedral bond angle. This deviation from the octahedral bond angle is the evidence for attaining "piano stool" geometry. In Complex **1**, the N(1)–C(17) bond length is 1.231 Å which is close to that of double bond character indicating the presence of NH proton which does not deprotonate in solution and also confirming the formation of a cationic complex. Also in complexes **2** and **5** the N(1)–C(17) bond length is close to that of a double bond character *i.e.,* 1.310–1.315 Å and the C(17)–N(2) bond length is around 1.347–1.349 Å which is close to a single bond character. This indicates the presence of NH proton, nevertheless the absence of counter ion in their molecular structure confirmed the formation of neutral monodentate complexes. In bidentate complexes **3**, **4**, **6** and **11** the bond length of C(17)–N(2) were found to be in the range of 1.298–1.308 Å which is close to that of a double bond character. This suggest the absent of acidic NH proton which deprotonate in solution forming a double bond C(17)–N(2) while the C(17)–N(1) bond length increases to 1.325–1.340 Å indicating the shifting of electron density towards N(1) where the C(17)–N(1) bond length is now converted to a single bond. The deprotonation of NH proton assists the benzothiazole ring to coordinate to the metal center as anionic ligands forming neutral bidentate complexes. The molecular structure of these complexes obtained clearly explicit the mode of bonding between the ligands and metals. From the crystal-packing diagram (Figure S23), the presence of hydrogen bonding interaction such as N–H, H–Cl and non-covalent interaction such as C–Cl between molecules in complexes **3** contribute to the overall stability of the complex. DCM which is the solvent of crystallization crystalized along with the complex and involved in two types of interaction. One of distance 2.609 Å involving interaction between nitrogen of the imine group of the ligand with one of the hydrogen atom of DCM. The other of distance 3.397 Å involving the carbon of the phenyl ring with one of the chlorine of DCM. Unfortunately, we could not obtain single crystal for triazolato complexes required for X-ray diffraction studies.

4. Conclusion

All together 21 new complexes have been synthesized. The ligands and complexes were characterized by spectroscopic techniques. Anti-bacterial studies for all the compounds have been carried out but none of them show any significant inhibition towards gram-positive and gram-negative bacteria. Versatility of benzothiazole hydrazone derivatives maybe attributed due to the presence of acidic NH proton. Substituents at para position of phenyl ring (H, F, CH_3) may also contribute to the versatility in the bonding modes of the benzothiazole hydrazone derivatives

Table 2
Selected bond lengths (Å) and bond angles (°) of complexes.

Complexes	1	2	3	4	5	6	11
M(1)–CNT	1.705	1.773	1.797	1.692	1.769	1.794	1.805
M(1)-Cl(1)	2.415(6)	2.4387(9)	2.3983(17)	2.4416(8)	2.4119(13)		
M(1)-Cl(2)	–	2.4039(9)	–	–	2.4096(9)	–	
M(1)-N(1)	2.121(17)	2.167(3)	2.083(5)	2.083(3)	2.161(3)	2.072(4)	2.063(9)
M(1)-N(3)	2.096(19)	–	2.113(6)	2.140(3)	–	2.126(4)	2.103(8)
M(1)-N(4)	–	–	–	–	–	–	2.131(9)
N(1)–C(17)	1.23(2)	1.309(4)	1.332(8)	1.340(4)	1.315(4)	1.325(6)	1.342(12)
N(2)–C(17)	1.34(2)	1.349(4)	1.308(8)	1.309(4)	1.347(4)	1.297(7)	1.325(12)
N(1)-M(1)-N(3)	75.4(7)	–	75.1(2)	76.16(11)	–	75.06(16)	76.2(3)
N(1)-M(1)-N(4)	–	–	–	–	–	–	86.5(3)
N(3)-M(1)-N(4)	–	–	–	–	–	–	86.2(3)
Cl(1)-M(1)-Cl(2)	–	87.58(3)	–	–	87.33(3)	–	
Cl(1)-M(1)-N(1)	83.1(5)	91.10(8)	85.83(14)	86.52(9)	91.47(7)	85.72(12)	
Cl(2)-M(1)-N(1)	–	92.79(8)	–	–	92.80(7)	–	
Cl(1)-M(1)-N(3)	83.9(5)	–	86.60(15)	86.28(8)	–	91.98(11)	

CNT represents the centroid of the *p*-cymene/Cp* ring and (M = Ru, Rh and Ir).

towards the metal centers especially in the case of rhodium complexes. Azido complexes of ruthenium and rhodium were found to be stable while triazolato complexes of rhodium were found to be unstable and decompose during separation. However triazolato complexes of ruthenium were found to be stable and their ^{1}H NMR clearly justified the formation of N(2) bound isomer. The single crystal X-ray diffraction study reveals the usual pseudo-octahedral "piano-stool" geometry of the complexes. Complexes of rhodium **2** and **5** bind preferentially through the benzothiazole nitrogen forming neutral mono-dentate complexes whereas their azido complexes bind to one azide anion and two nitrogen donor atoms of the chelating ligand forming neutral bidentate complex. In this complex the benzothiazole hydrazone derivatives undergo conformational switching from *E* to *Z* conformers. Thus, the introduction of sodium azide plays a vital role for the changes in conformation of the benzothiazole derivatives of monodentate rhodium complexes.

Acknowledgement

Lincoln Dkhar thanks DST-PURSE SCXRD, India for providing Single Crystal X-ray analysis and other spectral studies as well as DST INSPIRE for providing financial assistance in the form of university fellowship.

Appendix A. Supplementary data

Supplementary data to this article can be found online at https://doi.org/10.1016/j.jorganchem.2019.04.007.

References

[1] B. Therrien, Coord. Chem. Rev. 253 (2009) 493–519.
[2] A.L. Noffke, A. Habtemariam, A.M. Pizarro, P.J. Sadler, Chem. Commun. 48 (2012) 5219–5246.
[3] P. Govindaswamy, Y.A. Mozharivskyj, M.R. Kollipara, Polyhedron 26 (2007) 5039–5044.
[4] J.D. Blakemore, N.D. Schley, D. Balcells, J.F. Hull, G.W. Olack, C.D. Incarvito, O. Eisenstein, G.W. Brudvig, R.H. Crabtree, J. Am. Chem. Soc. 132 (2010) 16017–16029.
[5] D. Carmona, M. Lamata, L.A. Oro, Eur. J. Inorg. Chem. (2002) 2239–2251.
[6] O. Prakash, K.N. Sharma, H. Joshi, P.L. Gupta, A.K. Singh, Organometallics 33 (2014) 2535–2543.
[7] T. Ikariya, S. Kuwata, Y. Kayaki, Pure Appl. Chem. 82 (2010) 1471–1483.
[8] P. Zhang, P.J. Sadler, J. Organomet. Chem. 839 (2017) 5–14.
[9] S. Sarkar, A.A. Siddiqui, S.J. Saha, R. De, S. Mazumder, S. Banerjee, M.S. Iqbal, S. Nag, S. Adhikari, U. Bandyopadhyay, Antimicrob. Agents Chemother. 60 (2016) 4217–4228.
[10] P. Yadav, D. Chauhan, N.K. Sharma, S. Singhal, Int. J. Chem. Res. 2 (2010) 1209–1213.
[11] F.P. Mesquita, L.C. Pinto, B.M. Soares, A.J. de Sousa Portilho, E.L. da Silva, I.N. de Farias Ramos, A.S. Khayat, C.A. Moreira-Nunes, M.M. Bezerra, E. de Lucas Chazin, T.R.A. Vasconcelos, R.M.R. Burbano, M.E.A. de Moraes, R.C. Montenegro, Chem. Biol. Interact. 294 (2018) 118–127.
[12] X. Su, I. Aprahamian, Chem. Soc. Rev. 43 (2014) 1963–1981.
[13] S.L. Nongbri, B. Therrien, M.R. Kollipara, Inorg. Chim. Acta 376 (2011) 428–436.
[14] I.L. Mawnai, S. Adhikari, W. Kaminsky, M.R. Kollipara, J. Organomet. Chem. 869 (2018) 26–36.
[15] F. Ortega-Jiménez, J.G. Penieres-Carrillo, J.G. López-Cortés, M. Carmen Ortega-Alfaro, S. Lagunas Rivera, Chin. J. Chem. 35 (2017) 1881–1888.
[16] P.R.O. Crysalis, Version 1.171.36.20, release, Agilent Technologies, Yarnton, 2012.
[17] O.V. Dolomanov, L.J. Bourhis, R.J. Gildea, J.A.K. Howard, H. Puschmann, J. Appl. Crystallogr. 42 (2009) 339–341.
[18] G.M. Sheldrick, Acta Crystallogr. A71 (2015) 3–8.
[19] L.J. Bourhis, O.V. Dolomanov, R.J. Gildea, J.A.K. Howard, H. Puschmann, Acta Crystallogr. A71 (2015) 59–75.
[20] L.J. Farrugia, ORTEP-3 for windows -a version of ORTEP-III with a graphical user interface (GUI), J. Appl. Crystallogr. 30 (1997) 565.
[21] P. Govindaswamy, B. Therrien, G. Süss-Fink, P. Štěpnička, Ludvík, J. Organomet. Chem. 692 (2007) 1661–1671.
[22] R. Lalrempuia, M.R. Kollipara, P.J. Carroll, Polyhedron 22 (2003) 605–609.
[23] P. Paul, K. Nag, Inorg. Chem. 26 (1987) 2969–2974.
[24] A. Rosan, M. Rosenblum, J. Organomet. Chem. 80 (1974) 103–107.
[25] C.W. Chang, G.H. Lee, Organometallics 22 (2003) 3107–3116.
[26] T. Kemmerich, J.H. Nelson, N.E. Takach, H. Boehme, B. Jablonski, W. Beck, Inorg. Chem. 21 (1982) 1226–1232.
[27] A.P. Gaughan, K.S. Browman, Z. Dori, Inorg. Chem. 11 (1972) 601–608.
[28] W. Beck, K. Schropp, Chem. Ber. 108 (1975) 3317–3325.
[29] S.L. Nongbri, B. Das, M.R. Kollipara, J. Organomet. Chem. 694 (2009) 3881–3891.
[30] K.S. Singh, K.A. Kreisel, G.P.A. Yap, M.R. Kollipara, J. Organomet. Chem. 691 (2006) 3509–3518.
[31] P. Didier, I. Ortmans, A. Kirsch- De Mesmaeker, R. Watts, Inorg. Chem. 32 (1993) 5239–5245.
[32] B. Sullivan, D. Salmon, T. Meyer, Inorg. Chem. 17 (1978) 3334–3341.
[33] S. Adhikari, W. Kaminsky, M.R. Kollipara, J. Organomet. Chem. 836–837 (2017) 8–16.
[34] S. Adhikari, W. Kaminsky, M.R. Kollipara, J. Organomet. Chem. 848 (2017) 95–103.
[35] K. Jeyalakshmi, J. Haribabu, C. Balachandran, N.S.P. Bhuvanesh, N. Emi, R. Karvembu, New J. Chem. 41 (2017) 2672–2686.
[36] M.M. Sheeba, M.M. Tamizh, L.J. Farrugia, A. Endo, R. Karvembu, Organometallics 33 (2014) 540–550.